Biophysical Chemistry 23 (1985) 15-29
Elsevier

BPC 01021

DYNAMIC LIGHT SCATTERING STUDY OF SUSPENSIONS OF PURPLE MEMBRANE

Kenji KUBOTA [a], Yasunori TOMINAGA [a], Satoru FUJIME [b], Jun OTOMO [c] and Akira IKEGAMI [c]

[a] *Department of Physics, Faculty of Science, Ochanomizu University, Bunkyo-ku, Tokyo 112,* [b] *Mitsubishi-Kasei Institute of Life Sciences, Machida, Tokyo 194, and* [c] *The Institute of Physical and Chemical Research, 2-1 Hirosawa, Wako, Saitama 351, Japan*

Received 23rd April 1985
Revised manuscript received 28th May 1985
Accepted 15th June 1985

Key words: Dynamic light scattering; Purple membrane; Disc; Rotational diffusion; Anisotropic diffusion

Purple membrane from *Halobacterium halobium* in suspensions has been studied by quasielastic light scattering. The intensity correlation functions of polarized scattered light were measured at various K^2 values (K being the magnitude of the scattering vector), and the first cumulant $\bar{\Gamma}$ of the field correlation function $G^1(\tau)$ was obtained by a cumulant expansion method. The apparent diffusion coefficient $\bar{\Gamma}/K^2$ did not increase monotonically with K^2 values and showed a distinct anomaly in an intermediate range of K. A theoretical formulation of $G^1(\tau)$ for a disc and an extremely oblate ellipsoidal shell of revolution (S. Fujime and K. Kubota, Biophys. Chem. 23 (1985) 1) was applied to the analysis of the spectra, and characteristic features of experimental spectra were well reproduced. It was suggested that a strong interference effect between scattered rays on $\bar{\Gamma}/K^2$ should be attributed to a slight noncircular shape of the purple membrane and that a contribution to $\bar{\Gamma}/K^2$ from membrane flexibility should be taken into account. This study will provide experimental evidence of the feasibility of membrane studies by dynamic light scattering.

1. Introduction

Dynamic light scattering is one of the most powerful tools for studying dynamic and static structures of macromolecules [1,2]. This technique has become quite popular in the field of investigations of bio-macromolecules and organelles with the aid of recent advances in microelectronics. It has been successfully applied to various systems and has given enormously valuable information [3,4].

In the case where the scattering particles are small enough compared with $1/K$ ($K = (4\pi/\lambda)\sin(\theta/2)$; λ, wavelength of light in a medium; θ, scattering angle), the first cumulant $\bar{\Gamma}$ of the correlation function $G^1(\tau)$ gives the average translational diffusion coefficient of the particle. With the increase of the particle size, the dynamic structure factor includes the contribution from various higher-order modes, such as internal motion or rotation of the particle. When the shape of the particle is geometrically anisotropic, the coupling between translational and rotational diffusion becomes quite conspicuous and consideration of this coupling becomes essential to the analysis of the spectra of dynamic light scattering. A detailed study of this effect has been made for the case of a rigid rod system both theoretically [5] and experimentally [6]. In the cases of discs, where the radius is much larger than the thickness, and extremely oblate ellipsoids of revolution, the anisotropy in translational diffusion and the coupling effect should be as strong as those in the case of rods, and an interference effect between scattered rays should be stronger because of the two-dimensional nature of discs. Then, the spectrum of light scattered from such systems will be complicated in both static and dynamic aspects. To the best of

our knowledge, however, there are quite a few reports on theoretical and experimental studies of dynamic light scattering of a disc (or a disc-like particle). In the accompanying paper [7], we have presented a theoretical basis and formulations for the field correlation function $G^1(\tau)$ (and its first cumulant) from suspensions of rigid discs, ellipsoids and ellipsoidal shells of revolution. The results in that article will be applied to experimental results in this paper.

Yu et al. [8] studied the photoreceptor disc membrane isolated from bovine rod outer segments and determined its size and shape with elastic and quasi-elastic light scattering. They concluded that these segments are extremely homogeneous spherical vesicles which are derived from the native discs by osmotic swelling. Then, in their case, the effect of anisotropy in translational diffusion is quite small and the behavior of $\bar{\Gamma}/K^2$ as a function of K^2 is essentially similar to that of spheres. Packer et al. [9] studied the surface charge of purple membranes by use of laser Doppler velocimetry. Purple membrane shows orientational ordering in the presence of quite a low electric field (~ 10 V/cm), therefore the electrophoretic mobility is greatly influenced by anisotropy in translational diffusion. Therefore, knowledge of anisotropic diffusion is important.

In this paper, we investigated the spectrum of light quasielastically scattered from suspensions of purple membrane isolated from *Halobacterium halobium*. Purple membrane is present as specialized patches integrated within the cell membrane, and is a typical biomembrane. Purple membrane functions as light-energy converters and is composed of lipids and a single species of protein, bacteriorhodopsin [10]. Purified purple membrane can be suspended in the form of a sheet, the shape of which is very close to a disc. Its thickness is about 4.9 nm and diameter 0.5–0.6 μm. Thus, purple membrane is a very suitable material for a disc-like scatterer.

We first summarize the theoretical formulations of the field correlation function and of the first cumulant given in the accompanying paper [7]. Then, we will discuss experimental results, mainly the behavior of $\bar{\Gamma}/K^2$ as a function of K^2.

2. Theoretical section

2.1. Dynamic light scattering

First, we consider the amplitude of light scattered from a smooth rigid disc whose diameter and thickness are $2R$ and $2a$, respectively, and in which the mass distribution is uniform. In the following, we limit ourselves to the case of $Ka \ll 1$, and ignore the interference effect due to the finite thickness of the disc. The position vector $\boldsymbol{r}(t)$ of the surface element $\mathrm{d}S$ (the volume element being $2a\mathrm{d}S$) in the disc at time t is given by the relationship $\boldsymbol{r}(t) = \boldsymbol{R}(t) + \boldsymbol{j}(t)$, where $\boldsymbol{R}(t)$ is the position vector of the center-of-mass of the disc in the laboratory-fixed coordinate system and $\boldsymbol{j}(t)$ that of the surface element $\mathrm{d}S$ in the disc in the molecule-fixed coordinate system. Then, the amplitude of scattered light is proportional to

$$a(K, \xi, t) = \exp[i\boldsymbol{K}\cdot\boldsymbol{R}(t)] \times (1/\pi R^2)\iint \exp[i\boldsymbol{K}\cdot\boldsymbol{j}(t)]\,\mathrm{d}S \quad (1)$$

This integration is easily performed to give

$$a(K, \xi, t) = \exp[i\boldsymbol{K}\cdot\boldsymbol{R}(t)] \times [2J_1(Y)/Y] \quad (2)$$

where $J_1(z)$ is the first-order Bessel function, $\xi = \cos\theta$, $Y = KR\sin\theta = X(1-\xi^2)^{1/2}$ with $X = KR$ and θ the angle between the scattering vector $\boldsymbol{K}$ and the normal to the disc plane. The field correlation function of polarized scattered light is given by $G^1(\tau) = \langle a(K, \xi, t)a(-K, \xi', t')\rangle$, where $\tau = |t - t'|$ and $\langle \ldots \rangle$ denotes the statistical average. Then we have

$$G^1(\tau) = G_{\mathrm{D}}(\tau) \times \tfrac{1}{2}\iint [2J_1(Y)/Y] \times [2J_1(Y')/Y']\, g_{\mathrm{K}}(\xi, \xi'; \tau)\mathrm{d}\xi\,\mathrm{d}\xi' \quad (3)$$

where

$$G_{\mathrm{D}}(\tau) = \exp\left[-\left\{D_0 - \tfrac{1}{3}(D_3 - D_1)\right\}K^2\tau\right] = \exp(-D_1K^2\tau) \quad (4)$$

and $g_{\mathrm{K}}(\xi, \xi'; \tau)$ is the Green function which satisfies the following diffusion equation

$$\left[\partial/\partial\tau - \Theta\left(\nabla_\xi^2 - \mu^2\xi^2\right)\right] g_{\mathrm{K}}(\xi, \xi'; \tau) = \delta(\xi - \xi')\delta(\tau) \quad (5)$$

D_1 and D_3 are, respectively, translational diffusion coefficients parallel with and perpendicular to the disc plane, $D_0 = (2D_1 + D_3)/3$ the average translational diffusion coefficient, Θ the rotational diffusion coefficient around the diameter of the disc, $\mu^2 = (D_3 - D_1)K^2/\Theta$ the coupling constant between translational and rotational diffusion and $\nabla_\xi^2 = (\partial/\partial\xi)(1-\xi^2)(\partial/\partial\xi)$ the Laplace operator. Eq. 5 is easily solved by the method in ref. 5. By use of the previous result for $g_K(\xi, \xi'; \tau)$ [5,7], we have from eq. 3

$$G^1(\tau) = G_D(\tau)\sum_n\sum_m (2m+1) \times \left[\boldsymbol{U}\exp(-\Theta\boldsymbol{\Lambda}\tau)\boldsymbol{U}^{-1}\right]_{nm} a_n(X)a_m(X) \tag{6}$$

where the meanings of matrices $\boldsymbol{U}$ and $\boldsymbol{\Lambda}$ are given in refs. 5 and 7, and

$$a_n(X) = \int_0^1 \left[2J_1(Y)/Y\right] P_n(\xi)\mathrm{d}\xi \quad \text{(even } n\text{)}$$
$$= 0 \quad \text{(odd } n\text{)} \tag{7}$$

where $P_n(\xi)$ is the n-th order Legendre polynomial. If we ignore the anisotropy in translational diffusion, we have $[\boldsymbol{U}\exp(-\Theta\boldsymbol{\Lambda}\tau)\boldsymbol{U}^{-1}]_{nm} = \exp[-n(n+1)\Theta\tau]\delta_{nm}$. In this case, $(2n+1)a_n(X)^2$ gives the amplitude of the n-th mode.

In order to facilitate comparison of the theoretical formulation with experimental results, the first cumulant $\bar{\Gamma}$ of $G^1(\tau)$ has been derived by use of a relationship $\bar{\Gamma} = -(\partial/\partial\tau)\ln G^1(\tau)|_{\tau=0}$;

$$\bar{\Gamma}/K^2 = \left[D_0 - \tfrac{1}{3}(D_3 - D_1)\right] + \langle R_g^2\rangle\Theta g_1(X) + (D_3 - D_1)g_2(X) \tag{8}$$

where $\langle R_g^2\rangle$ is the mean square radius of gyration around the diameter of the disc; $\langle R_g^2\rangle = R^2/4$ for a thin disc. Functions $g_1(X)$ and $g_2(X)$ are given by

$$g_1(X) = \left(1/\langle R_g^2\rangle K^2\right)\sum_n n(n+1) \times (2n+1)a_n(X)^2/G^1(0) \tag{9}$$

$$g_2(X) = \sum_n (2n+1)a_n(X)\left[L_0(n)a_n(X) + L_2(n-2)a_{n-2}(X) + L_1(n+2)a_{n+2}(X)\right]/G^1(0) \tag{10}$$

where $G^1(0) = \Sigma(2n+1)a_n(X)^2$ is the static scattering intensity and

$$L_0(n) = (2n^2 + 2n - 1)/(2n-1)/(2n+3)$$
$$L_1(n) = n(n-1)/(2n-1)/(2n-3) \tag{11}$$
$$L_2(n) = (n+1)(n+2)/(2n+3)/(2n+5)$$

Next, we consider an extremely oblate ellipsoidal shell of revolution. For an ellipsoidal shell of revolution

$$(x^2 + y^2)/R^2 + z^2/a^2 = 1 \tag{12}$$

we have [12]

$$a(K, \xi, t) = \exp\left[i\boldsymbol{K}\cdot\boldsymbol{R}(t)\right] \times j_0(Z) \tag{13}$$

where $j_0(z) = (\sin z)/z$ is the zeroth-order spherical Bessel function, $Z = KR(1 - q\xi^2)^{1/2}$, $q = 1 - p^{-2}$ and $p = R/a$ the axial ratio. For an extremely oblate ellipsoidal shell, we have

$$Z = KR\sin\theta = X\sin\theta \quad (R \gg a) \tag{14}$$

The dynamic form factors are given by (cf. eq. 7)

$$d_n^s(X) = \int_0^1 j_0(Z)P_n(\xi)\mathrm{d}\xi \quad \text{(even } n\text{)}$$
$$= 0 \quad \text{(odd } n\text{)} \tag{15}$$

The radius of gyration of an extremely oblate ellipsoidal shell of revolution is given by $\langle R_g^2\rangle = R^2/3$, and we have

$$\bar{\Gamma}/K^2 = \left[D_0 - \tfrac{1}{3}(D_3 - D_1)\right] + (R^2/3)\Theta g_1(X) + (D_3 - D_1)g_2(X) \tag{16}$$

where $g_1(X)$ and $g_2(X)$ are given by eqs. 9 and 10 with replacement of $a_n(X)$ with $d_n^s(X)$, respectively.

The numerical method for evaluating $a_n(X)$ and $d_n^s(X)$ is detailed in the accompanying paper [7].

2.2. Diffusion coefficients

Theoretical formulations for the diffusion coefficients of discs have not yet been reported. Those for an ellipsoid of revolution, however, have been given by Perrin [13]. According to his theory, diffusion coefficients of extremely oblate ellipsoid and ellipsoidal shell of revolution with the major axis $2R(\gg 2a)$ are given by

$$\begin{aligned} D_0 &= k_B T/12\eta R \\ D_1 &= 3k_B T/32\eta R \\ D_3 &= k_B T/16\eta R \\ \Theta &= 3k_B T/32\eta R^3 \end{aligned} \tag{17}$$

where η is the viscosity of the medium, k_B the Boltzmann constant and T the absolute temperature. Eq. 17 has some characteristic features: For $R \gg a$, diffusion coefficients are independent of the 'thickness' a. Also, correction terms due to the end effect do not appear explicitly in eq. 17. These make a striking contrast to the case of a rigid rod.

3. Experimental section

3.1. Preparation of purple membrane

Purple membrane was purified from *H. halobium* Et1001. The culture conditions and purification procedures were essentially the same as those of Oesterhelt and Stoeckenius [14]. Purification of the preparation was examined by SDS-polyacrylamide gel electrophoresis and a single peak was obtained.

Purple membrane obtained as above still has a broad size distribution. To make the distribution narrower, we followed essentially the same method as that of Kimura et al. [15]. Purple membrane was suspended in 5 mM Hepes buffer solution at pH 7.1. The concentration of purple membrane in suspension was determined from measurement of the absorbance. For the light-scattering measurements, the stock suspension was diluted carefully without giving unnecessary shear flow in order not to break the membrane, and the preparation was stored in a refrigerator until use. All measurements were carried out within 2–3 days after the final dilution. The purple membrane suspension was filtered through a Millipore filter of 0.8 μm pore size directly into a scattering cell, which was a 10 mm outer diameter polished cylindrical cell and was thoroughly washed and rinsed with the buffer solution.

Fig. 1 shows a typical picture of purple membranes taken by A. Tomioka (personal communication) for the same preparation as ours before filtration. The shape of most purple membranes is close to a circular sheet with diameter 0.4–0.7 μm. Some are more or less elliptic. The size distribution seems to be relatively narrow.

3.2. Light scattering

Light-scattering measurements were carried out with a home-made spectrometer and a real-time 252-channel single clipped digital correlator. Details of this system have been described elsewhere [6]. We used an argon ion laser (GLG-3200, NEC) operating at 488.0 nm with a power less than 5 mW at the position of the sample cell. This wavelength lies within the absorption band of bacteriorhodopsin and the photoreaction cycle could be activated. However, Doppler velocimetry with a 632.8 nm beam has shown that at pH 7.0, no detectable light-induced changes in surface charge are observed unless the purple membrane preparation is chemically modified, such as nitration [9]. Since the absorption coefficient at 488.0 nm is almost the same as that at 632.8 nm [14], we can expect that the change in surface charge in-

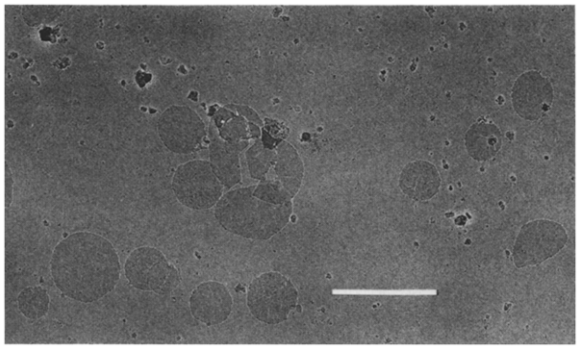

Fig. 1. Rotary shadow-cast images of purple membranes. Scale bar: 1 μm.

duced by the probe light beam could be minimized enough under the above experimental condition. The temperature was regulated within ±0.02°C at 15–40°C.

Theoretically, $G^1(\tau)$ is expressed as a sum of many exponentials. Due to the relatively large sizes of purple membranes, a strong interference effect and a still present size distribution, however, decomposition of the experimental $G^1(\tau)$ into a sum of exponentials is difficult and not practical. In such a case, the most characteristic measure of the correlation function will be given by the average decay rate or the first cumulant $\bar{\Gamma}$. The experimental intensity correlation functions were analyzed by a cumulant expansion method [16] up to a third order to obtain the reliable first cumulant. Fitting was performed by a least-squares method applied to

$$G^1(\tau)/G^1(0) = \exp(-\bar{\Gamma}\tau)\left[1 + (\mu_2/2!)\tau^2 - (\mu_3/3!)\tau^3 + \ldots\right] \quad (18)$$

where μ_i is the i-th moment around $\bar{\Gamma}$ of the decay rate distribution and $\mu_2/\bar{\Gamma}^2$ gives normalized dispersion.

4. Results and discussion

In this paper, results are reported for two preparations, sample A at a concentration of 13.1 μg/ml and sample B at 25.6 μg/ml, both in 5 mM Hepes buffer solution at pH 7.1. These concentrations are sufficiently dilute so that the interaction between purple membranes does not contribute [15]. And it is not necessary to consider the concentration dependence of correlation function profiles. Our preparation was inferred to have a relatively narrow size distribution as shown in fig. 1, but the average size of the membrane was different from one batch to another, though the overall characteristics were quite similar as shown below.

4.1. Cumulant analysis

The results of the third-order cumulant expansion of correlation functions for samples A and B at 25°C are shown in figs. 2 and 3, respectively.

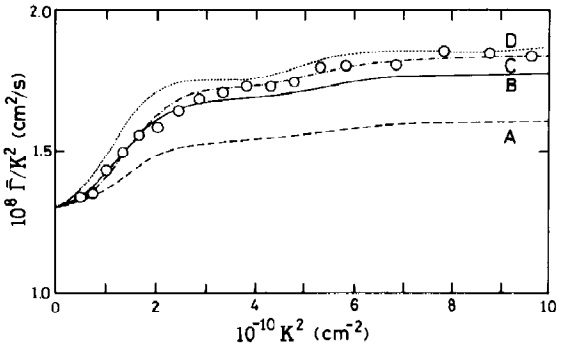

Fig. 2. The $\bar{\Gamma}/K^2$ vs. K^2 relationship of sample A at 25°C in 5 mM Hepes buffer (pH 7.1). The concentration is 13.1 μg/ml. Hollow circles show the experimental results. Curve A (– – –) denotes the theoretically reconstructed curve with $D_0 = 1.298$, $D_1 = 1.458$, $D_3 = 0.979$ and $(D_3 - D_1) = -0.479$ in units of 10^{-8} cm²/s and $\Theta = 16.9\ s^{-1}$, which are the Perrin values for $R = 295$ nm and $a = 2.45$ nm. Curve B (———) denotes the theoretically reconstructed curve to fit with experimental results at low scattering angles; $\Theta = 22\ s^{-1}$ and D_i ($i = 0$, 1 and 3) being the same as those for curve A. Curve C (– · – · –) denotes the result of a least-squares fit to eq. 8 for the given value of $D_0 = 1.298 \times 10^{-8}$ cm²/s; the best-fit parameter values are $(D_3 - D_1) = -0.917 \times 10^{-8}$ cm²/s and $\Theta = 31.1\ s^{-1}$. Curve D (------) denotes the theoretically reconstructed curve for $D_0 = 1.298 \times 10^{-8}$ cm²/s and $\Theta = 16.9\ s^{-1}$, where $D_3 = D_1$ is tentatively assumed.

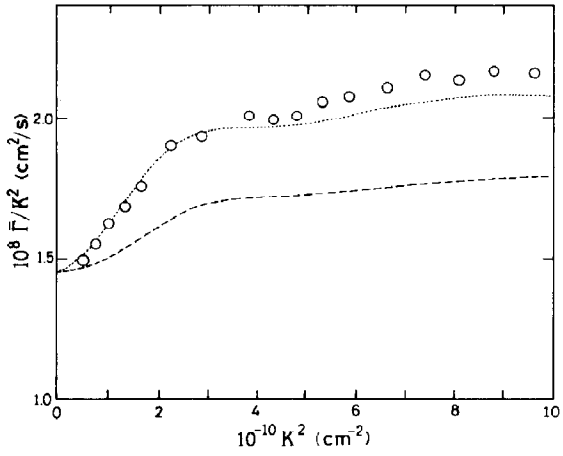

Fig. 3. The $\bar{\Gamma}/K^2$ vs. K^2 relationship of sample B at 25°C in 5 mM Hepes buffer (pH 7.1). The concentration is 25.6 μg/ml. (– – –) Theoretically reconstructed curve with $D_0 = 1.450$, $D_1 = 1.628$, $D_3 = 1.094$ and $(D_3 - D_1) = -0.534$ in units of 10^{-8} cm²/s and $\Theta = 23.4\ s^{-1}$, which are the Perrin values for $R = 264.6$ nm. (------) Theoretically reconstructed curve where $D_3 = D_1$ is tentatively assumed.

The K^2 range was 0.55–10 in units of 10^{10} cm^{-2}. The standard deviation in the $\bar{\Gamma}/K^2$ values was about 2%. The normalized dispersion $\mu_2/\bar{\Gamma}^2$ was about 0.1 at low scattering angles and increased at higher angles. The quality of the least-squares fitting was monitored by the correlation coefficient of the deviations of the fitted function from the measured one [6], and the correlation coefficient was large enough to indicate that the deviations were quite random. The most striking feature of the results shown in figs. 2 and 3 is that $\bar{\Gamma}/K^2$ does not increase monotonically with K^2 and shows distinct anomaly (wiggling) in an intermediate range of K^2. This is quite in contrast to the results for a rigid rod [6] and a semiflexible filament [17]. This wiggling in $\bar{\Gamma}/K^2$ values existed in both samples A and B and many other preparations not shown here, and is concluded not to be due to any artifact introduced in experimental procedures.

From the low-angle values of $\bar{\Gamma}/K^2$, the average translational diffusion coefficient $\langle D_0 \rangle_h^o$ was determined to be $(1.30 \pm 0.03) \times 10^{-8}$ cm^2/s for sample A, where $\langle \ldots \rangle_h^o$ denotes the light-scattering ('h') value at $K^2 = 0$ ('o') averaged over a size distribution ('$\langle\rangle$'), i.e., the so-called z-average. Using this value of D_0 and the Perrin's formula for D_0 (eq. 17), we obtained the average radius of the purple membrane of sample A as 295 nm. Similarly, from a D_0 value of $(1.45 \pm 0.03) \times 10^{-8}$ cm^2/s for sample B, an average radius of 274 nm was obtained. These values of radii are quite compatible with disc-like images on electron micrographs. Then, eq. 17 permits one to estimate D_1, D_3, and Θ, which are 1.458×10^{-8} cm^2/s, 0.979×10^{-8} cm^2/s and 16.9 s^{-1} for sample A, respectively, and 1.628×10^{-8} cm^2/s, 1.094×10^{-8} cm^2/s and 23.4 s^{-1} for sample B, respectively. With these transport coefficients, theoretical curves for $\bar{\Gamma}/K^2$ as a function of K^2 can be calculated.

Table 1
Numerical values of $g_1(KR)$ and $g_2(KR)$ for a disc

KR	$g_1(KR)/2$	$g_2(KR)$	KR	$g_1(KR)/2$	$g_2(KR)$
0.0	0.00000	0.33333	5.2	0.61705	0.79473
0.2	0.00067	0.33422	5.4	0.61825	0.79039
0.4	0.00270	0.33692	5.6	0.62196	0.79031
0.6	0.00616	0.34147	5.8	0.62845	0.79486
0.8	0.01117	0.34799	6.0	0.63896	0.80380
1.0	0.01790	0.35663	6.2	0.65308	0.81639
1.2	0.02660	0.36759	6.4	0.67010	0.83144
1.4	0.03757	0.38110	6.6	0.68886	0.84743
1.6	0.05119	0.39746	6.8	0.70787	0.86270
1.8	0.06794	0.41700	7.0	0.72553	0.87564
2.0	0.08837	0.44008	7.2	0.74040	0.88499
2.2	0.11310	0.46704	7.4	0.75147	0.89008
2.4	0.14278	0.49816	7.6	0.75842	0.89099
2.6	0.17800	0.53353	7.8	0.76156	0.88845
2.8	0.21916	0.57293	8.0	0.76181	0.88368
3.0	0.26621	0.61559	8.2	0.76039	0.87810
3.2	0.31837	0.66006	8.4	0.75862	0.87308
3.4	0.37390	0.70404	8.6	0.75766	0.86973
3.6	0.42993	0.74456	8.8	0.75841	0.86878
3.8	0.48283	0.77844	9.0	0.76140	0.87056
4.0	0.52884	0.80308	9.2	0.76680	0.87501
4.2	0.56514	0.81731	9.4	0.77440	0.88170
4.4	0.59060	0.82177	9.6	0.78366	0.88988
4.6	0.60601	0.81868	9.8	0.79379	0.89863
4.8	0.61360	0.81113	10.0	0.80386	0.90691
5.0	0.61631	0.80227	∞	1.0	1.0

For this purpose, the numerical values of $g_1(X)$ and $g_2(X)$ in eq. 8 have to be computed according to eqs. 9 and 10. The computed values are tabulated in table 1 and shown graphically in fig. 4. These curves should be compared with those in fig. 3 for a rod in the accompanying paper [7] and show remarkable wiggling due to a strong interference effect between scattered rays from a disc. With these values of g_1 and g_2, theoretical curves were computed and are shown in figs. 2 and 3. In both theoretical curves, distinct wiggling is noticed at around $K^2 \simeq 4 \times 10^{10}$ cm^{-2}; these positions correspond quite well to those of the experimental ones. However, the magnitude of $\bar{\Gamma}/K^2$ values of the theoretical curve is much smaller than the experimental one for both samples A and B. If no anisotropy in translational diffusion is tentatively assumed, i.e., $D_3 = D_1$, we have

$$\bar{\Gamma}/K^2 = D_0 + (R^2/4)\Theta g_1(X)$$

This relation is also shown in figs. 2 and 3 for the Perrin values of D_0 and Θ for samples A and B, respectively. Although the curves for $D_3 = D_1$ show better fitting to the experimental results than those for $D_3 \neq D_1$ for both samples, we cannot accept these cases. The reason for this came from our experimental result for dilute suspensions of tobacco mosaic virus, which clearly indicated a very large effect of anisotropy in translational diffusion on both $\bar{\Gamma}/K^2$ values and profiles of $G^1(\tau)$ [6]. The theoretical $\bar{\Gamma}/K^2$ values (for $D_3 = D_1$) averaged over a size distribution of the preparation will become appreciably larger than the experimental ones as inferred from discussion given later. The membrane flexibility, if present, will also result in larger $\bar{\Gamma}/K^2$ values. These implicitly suggest the contribution of anisotropy in translational diffusion to the present result as well.

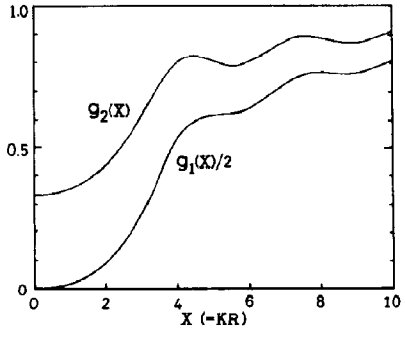

Fig. 4. Graphic representation of $g_1(KR)$ and $g_2(KR)$ for a thin disc as a function of KR. Both $g_1(KR)/2$ and $g_2(KR)$ tend toward unity as $KR \to \infty$.

Several reasons are possible for the discrepancies between experimental $\bar{\Gamma}/K^2$ values and the theoretical ones for a rigid disc with the Perrin values of D_i ($i = 0$, 1 and 3) and Θ. One is that the theoretical curve corresponds to that for a monodisperse preparation of discs, but the actual preparation still has a size distribution and every purple membrane is not perfectly circular. The other reason is that purple membrane may not be rigid and has some degree of flexibility, which would contribute to the $\bar{\Gamma}/K^2$ values. These will be discussed below.

4.2. Effect of flexibility

We first examined the effect of the membrane flexibility. Though the formulation of the correlation function for a weakly bending rod including flexing motion has already been reported and well discussed [17], the formulation for a weakly bend-

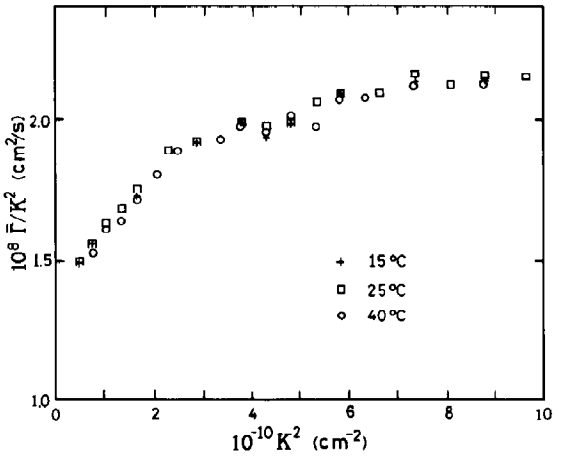

Fig. 5. The $\bar{\Gamma}/K^2$ vs. K^2 relationships of correlation functions measured at 15°C (+), 25°C (□) and 40°C (○) after T/η correction to 25°C. Sample B at the same solvent condition as in fig. 3. Three data coincide with each other within experimental error.

ing disc is still lacking. Therefore, we examined the effect of flexibility by an indirect method. When the flexibility depends on temperature, the correlation function cannot scale with T/η, and $\bar{\Gamma}/K^2$ after T/η correction should show a deviation from that measured at different temperature. This has been clearly shown in the case of muscle thin filaments [18,19]. In the case of fd virus, on the other hand, the experimental correlation functions for dilute suspensions have been known to scale with T/η [18] though this filament has appreciable flexibility [17]. Namely, T/η scaling holds for a scatterer with a temperature-independent nonzero flexibility parameter as well as for a rigid scatterer [20].

The $\bar{\Gamma}/K^2$ values of correlation functions measured at 15, 25 and 40°C are shown in fig. 5 after T/η correction to 25°C for sample B. All of the data points coincide with each other within experimental error. It is noteworthy that wiggling is clearly observed at all temperatures. The scaling was also examined for the correlation functions themselves. This is shown in fig. 6, where the correlation functions were measured at the scattering angle of 120° and at 15 and 25°C. In this figure, the correlation function measured at 15°C was fitted to that at 25°C with only one adjustable parameter; the magnitudes of the first channel were equated with each other. The agreement is quite good again. Then, T/η scaling was confirmed and the contribution from flexibility to the spectra could not be asserted positively by the present method. But, when the solvent condition was changed from pH 7.1 to 11.5, the $\bar{\Gamma}/K^2$ value

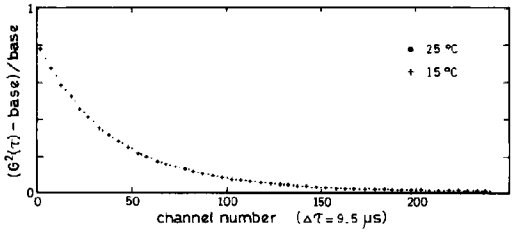

Fig. 6. Net correlation function profiles at the scattering angle of 120° for sample B measured at 15°C (+) and 25°C (●). After T/η correction of the delay time to that at 25°C, the amplitude of the correlation function at 15°C was scaled so that the value of the first channel became equal to that at 25°C.

for sample B at $K^2 = 5.87 \times 10^{10}$ cm^{-2} ($\theta = 90°$), for example, changed drastically from 2.07 to 2.60 in units of 10^{-8} cm^2/s, and the whole curve shifted upwards without changing the $\bar{\Gamma}/K^2$ value extrapolated to $K^2 = 0$. This might suggest a change in the flexibility with solvent conditions, because aggregation and/or decomposition, i.e., the change in size distribution, should also cause the change in the D_0 value, and the $\bar{\Gamma}/K^2$ value extrapolated to $K^2 = 0$ should change. Then, we may possibly say that the purple membrane is not a rigid disc and has some degree of flexibility though it may not be large under moderate conditions. A theoretical formulation for a flexible disc is very desirable.

4.3. *Effect of size distribution*

We considered a possible effect of the size distribution on $\bar{\Gamma}/K^2$ values. If we use the $\langle D_0 \rangle_h^\circ$ values in eq. 8, the corresponding values of D_1 and D_3 should be $\langle D_1 \rangle_h^\circ$ and $\langle D_3 \rangle_h^\circ$, respectively. But the meaning of the average of Θ should be different from those of D_i because of its different dependence on radius. Moreover, both $\langle D_i \rangle_h$ and $\langle \Theta \rangle_h$ will depend on K^2 for a polydisperse preparation. In order to examine this situation, we analyzed the correlation functions by several methods. The first one is the analysis of $\bar{\Gamma}/K^2$ at low angles by eq. 8, because it is expected that the contribution of flexing motion is possibly negligible at low angles. The second is a two-exponential analysis of the correlation functions and extraction of the apparent rotational diffusion coefficient. And the third possibility is to determine the size distribution from the determination of the distribution of decay rates of the correlation function itself. The third method is usually the most reliable for determining the size distribution [21]. Unfortunately, however, this method was not applicable: In the present particular case of purple membranes of a large size, even at relatively low angles not only the purely translational mode but also higher modes, which include the contribution of rotational diffusion, contribute to the correlation function. This situation is shown in fig. 7. Here, the amplitude factors, $(2n+1)a_n(X)^2$ (see section 2), in the absence of anisotropy in translational

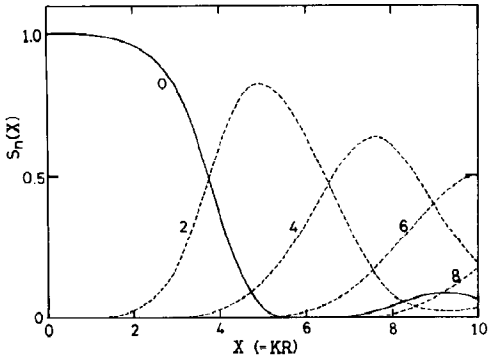

Fig. 7. Graphic representation of the amplitudes $S_n(KR) = (2n+1)a_n(KR)^2$ for a thin disc in the absence of anisotropy in translational diffusion. In this plot, amplitudes are normalized as $\Sigma_n S_n(KR) = 1$ for any KR value. (Amplitudes $P_n(KR)$ in the presence of anisotropy are different from $S_n(KR)$; for details, see ref. 7.)

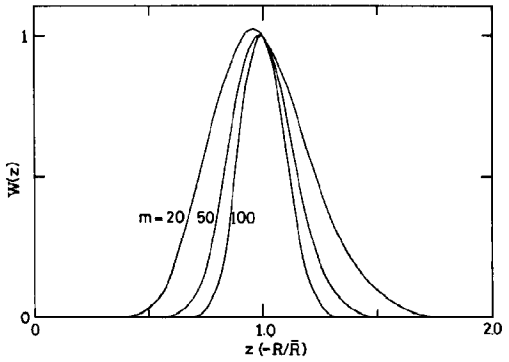

Fig. 8. The profile of the Schulz-Zimm distribution function. The number beside each curve represents the polydispersity parameter m. All the curves were normalized as $W(\bar{R}) = 1$.

diffusion are shown, which are modified in the presence of anisotropy (see ref. 7). For $R = 295$ nm at a scattering angle of 45°, the KR value is 3.87 and not only $n = 0$ and $n = 2$ modes but also the $n = 4$ mode already contribute to the correlation function. Or, even at 25° or $KR = 2.19$, the $n = 2$ mode contributes appreciably. Therefore, the analysis of the distribution of decay rates of the correlation functions is quite complicated and seems not to be practical. Then, we assumed an analytical distribution function and examined the behavior of $\bar{\Gamma}/K^2$ as a function of K^2 including polydispersity. The postulated size distribution function was the Schulz-Zimm distribution function because of its mathematical tractability and a broad applicability to a polydisperse system [22–24];

$$W(R)\mathrm{d}R = (1/m!)(m+1)^{m+1}(R/\bar{R})^m \times \exp[-(m+1)R/\bar{R}]\mathrm{d}(R/\bar{R}) \quad (19)$$

where $W(R)$ is the number fraction of discs having radii in the range R to $R + \mathrm{d}R$, $\bar{R}$ the number-average radius and m the measure of polydispersity. The monodisperse distribution is given by $m = \infty$. The profiles of distribution for several values of m are shown in fig. 8. For these distributions, theoretical $\bar{\Gamma}/K^2$ curves were calculated with the Perrin value of the radius 295 nm for sample A and are shown in fig. 9 (see appendix for algorithm of simulation). It should be noted that wiggling at the intermediate range of K^2 suffers

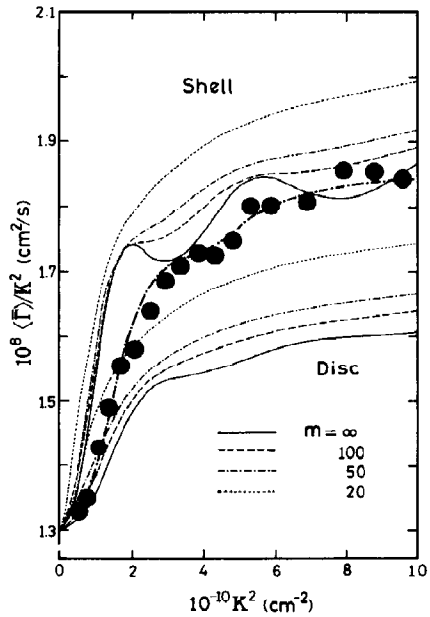

Fig. 9. The theoretical curves of $\langle\bar{\Gamma}\rangle/K^2$ as a function of K^2 for a disc (Disc) and an extremely oblate ellipsoidal shell of revolution (Shell) with size distributions. All the curves were reconstructed with $\langle D_0\rangle_h^0 = 1.298\times10^{-8}$ cm²/s or $\langle 1/R\rangle_h^0 = (295\text{ nm})^{-1}$. Filled circles and the thick dot-dashed line are taken from fig. 2 for a comparison. For algorithm of computation, see appendix.

from polydispersity, and even for $m = 100$ the wiggling is almost extinguished. Moreover, for a relatively broad distribution of $m = 20$, the theoretical $\bar{\Gamma}/K^2$ value is 1.74×10^{-8} cm^2/s at $K^2 = 10 \times 10^{10}$ cm^{-2} and still smaller than the experimental one of 1.84×10^{-8} cm^2/s. These two points suggest that the behavior of $\bar{\Gamma}/K^2$ cannot be explained by a model for a rigid disc with a size distribution alone. This is also shown by the first two methods of the analysis mentioned above: After the first method, the $\bar{\Gamma}/K^2$ values for $K^2 \leqslant 2.5 \times 10^{10}$ cm^{-2} were least-squares fitted to eq. 8 with only Θ being floated, and $\Theta = 22$ s^{-1} was obtained. Using this Θ value, the theoretical curve of $\bar{\Gamma}/K^2$ was again calculated, and the result is shown in fig. 2 by the solid curve. The overall feature is quite similar to the experimental one, and the position and behavior of wiggling are reproduced quite well. There still remains, however, a discrepancy in size at larger K^2 values. This again suggests the possible presence of flexing motion, because the value of $\Theta = 22$ s^{-1} is compatible with the result from the second method: A two-exponential analysis was carried out for the correlation function, for example, at a scattering angle of 35°. At this scattering angle, the KR value is 3.04 for $R = 295$ nm and small enough so that it is not necessary to include the contribution from the $m = 4$ mode according to fig. 7. The resultant Θ value was 23.5 s^{-1}, which was determined from the relationship $\Theta = (\Gamma_2 - \Gamma_0)/6$ where Γ_0 and Γ_2 are, respectively, the slow and fast decay rates of the correlation function.

We further analyzed the $\bar{\Gamma}/K^2$ values by the least-squares fit to eq. 8 with both Θ and $(D_3 - D_1)$ being floated. This analysis gave $\Theta = 31.3$ s^{-1} and $(D_3 - D_1) = -0.917 \times 10^{-8}$ cm^2/s. The fitting was very good (see fig. 2), but the value of $(D_3 - D_1)$ was almost twice as large as that estimated from Perrin's formulas for a monodisperse preparation, and seemed to be quite unreasonable. This came from the fact that experimental excess values of $\bar{\Gamma}/K^2 - \langle D_0 \rangle_h^\circ$ are much larger than theoretical ones for a disc with $\langle 1/R \rangle_h^\circ = (295 \text{ nm})^{-1}$ (see fig. 9). The model for a rigid disc alone can well explain characteristic features of experimental results qualitatively but not quantitatively, even when sample polydispersity is taken into account. Apart from the membrane flexibility, therefore, we have to seek another possibility.

4.4. Effect of noncircular shape

We examined the effect of the noncircular shape of purple membrane on the spectra. As seen in fig. 1, the shape of the purple membrane is more or less elliptic. Due to the decrease in symmetry in shape of the scatterer, a theoretical formulation of the correlation function for an elliptic sheet becomes quite complicated, and may not be practical even if possible. Therefore, we adopted an approximate method for the estimation of the effect of noncircular shapes of the scatterers, i.e. we regard an elliptic sheet (and a disc with a little irregular circumference) as a disc with an extra mass at its circumference. Of course, this is a very rough approximation, but the interference effect between scattered rays from an actual scatterer could be retrieved. A simple model for a disc with an extra mass at its circumference is a disc plus ring system [7] or an extremely oblate ellipsoidal shell of revolution. We adopted here the latter model, where the radial mass density is reasonably constant near the center and increases at the circumference as shown in fig. 10. In this model of an ellipsoidal shell, Perrin's formulas hold for the estimation of transport coefficients. The theoretical values of $g_1(X)$ and $g_2(X)$ for an ellipsoidal shell were calculated and are shown in fig. 11. This should be compared with fig. 4. Due to the interference effect between scattered rays from the extra mass, the oscillatory behavior of g_1 and g_2 becomes greatly emphasized and wiggling appears

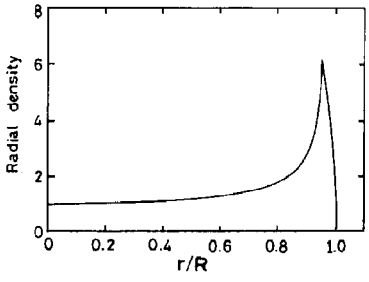

Fig. 10. Radial mass density of an ellipsoidal shell of revolution with the ratio of axes of outer and inner ellipsoid being 0.95.

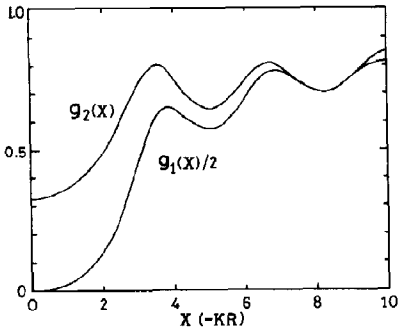

Fig. 11. Graphic representation of $g_1(KR)$ and $g_2(KR)$ as a function of KR for an extremely oblate ellipsoidal shell of revolution.

even at smaller KR values than in the case of a disc, though the behavior at sufficiently small KR values is very similar. For an ellipsoidal shell with $R = 295$ nm corresponding to sample A, the theoretical $\bar{\Gamma}/K^2$ vs. K^2 relationship was calculated and is shown in fig. 9 ($m = \infty$). Comparing with that for a disc with $m = \infty$, the magnitude of $\bar{\Gamma}/K^2$ values increased remarkably (mainly due to a larger value of $\langle R_g^2 \rangle$; $R^2/3$ instead of $R^2/4$ for a disc) and wiggling in $\bar{\Gamma}/K^2$ is greatly emphasized. The value of K^2, where wiggling first appears, becomes smaller. Moreover, with the postulated size distribution shown in fig. 8, the behavior of $\bar{\Gamma}/K^2$ with polydispersity was calculated and is also shown in fig. 9. It should be noted that wiggling is present even for $m = 50$ in contrast to the case of a disc. These points, that the magnitude of the $\bar{\Gamma}/K^2$ value is larger and wiggling suffers less from polydispersity than those of a disc, are very compatible with the experimental results. A blend of two models for a disc and a shell with a certain weight could work very well for the present situation of membrane preparations.

Here it is interesting to examine the effect of a noncircular shape of the scatterer on diffusion coefficients. For an extremely oblate ellipsoid $x^2/R^2 + y^2/R'^2 + z^2/a^2 = 1$ with $R = 330$ nm, $R' = 264$ nm and $a = 2.45$ nm (the same thickness and sectional area as those of a disc with thickness $2a = 4.5$ nm and $R = 295$ nm), Perrin's formulas [13] give $D_0 = 1.394$, $(D_1 + D_2)/2 = 1.565$ and $D_3 = 1.051$ in units of 10^{-8} cm^2/s and $\Theta = 18.3$ s^{-1}. The Θ value is the average of those around the x- and y-axes. The values of diffusion coefficients for the ellipsoid become larger than those of the disc. Another example is that for an ellipsoid with $R = 295$ nm, $R' = 236$ nm and $a = 2.45$ nm, $\Theta = 21.1$ s^{-1} is calculated. These two examples suggest that the effect of a noncircular shape of the scatterer will modify the diffusion coefficients and may increase those values. Since we do not know the exact extent of noncircularity and its distribution, we do not proceed further, but may say that the difference between the Perrin value of $\Theta = 16.9$ s^{-1} and the above results of $\Theta = 22$ and 23.5 s^{-1} will also be diminished more or less by noncircularity of the scatterer's shape.

4.5. Static intensity

We now turn to the results of static intensity measurements. The form factor $P(\theta)$ of a thin disc is expressed by $(2/X^2)(1 - J_1(2X)/X)$ where $X = KR$. Since $P(\theta)$ is proportional to $I(\theta)$ in the case of small optical anisotropy, the K^2-weighted intensity of scattered light, $\sin^2(\theta/2)I(\theta)$, is a simple function of KR or K^2. This is shown in fig. 12 for sample A. In this plot the oscillatory feature of the intensity becomes clear. Theoretically predicted profiles for suspensions of discs and extremely oblate ellipsoidal shells of radius 295 nm are also shown. In the case of purple membranes, the optical anisotropy may not be small and the measured polarized scattered intensity, I_{vv}, also includes the contribution from the depolarized scattered intensity, and is not directly proportional to $P(\theta)$. However, since the angular dependence of the depolarized component is generally very weak, the oscillatory profile will remain almost unchanged. Then, the comparison of $\sin^2(\theta/2)I(\theta)$ with the theoretical one is still meaningful. As shown in fig. 12, general features in the experimental profile and the theoretical one for a disc are in good agreement. In the case of an ellipsoidal shell, the oscillatory pattern is much more emphasized than that for a disc and $\sin^2(\theta/2)I(\theta)$ seems to increase as a whole with the increase of K^2. These again suggest that the scattering profile of purple membranes is well explained by a blend of models for a disc and an extremely oblate ellipsoidal shell.

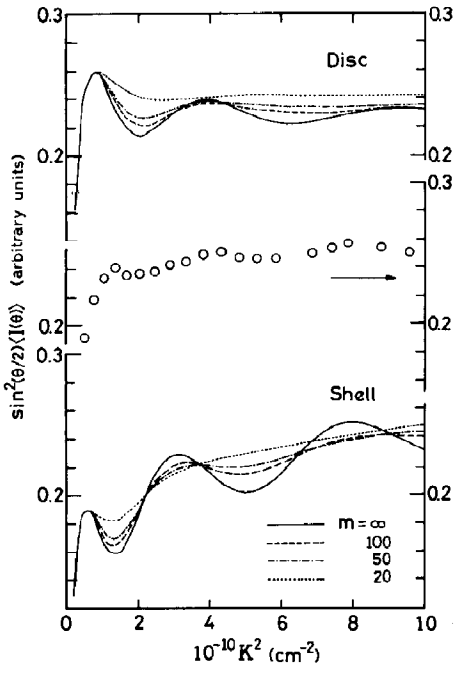

Fig. 12. The static scattering intensity $\sin^2(\theta/2)\langle I(\theta)\rangle$ as a function of K^2. The hollow circles denote the experimental results for sample A. The theoretical curves were computed for $\langle 1/R\rangle_h^o = (295\ \text{nm})^{-1}$. For details of algorithm, see appendix.

4.6. Future perspectives

Norisuye and Yu [12] investigated isolated rod discs by light scattering, and observed osmotically induced deformation. They argued that the results are well explained by a model based on an ellipsoidal shell (and a spherical shell as a limiting form of the former). The scattered intensity profile depends on the axial ratio and shows a characteristic pattern. An analysis of intensity profiles is useful for the characterization of such systems as they studied. They also observed the photoinduced deformation. In this respect, the following should be noteworthy. Purple membrane has net charges and a permanent dipole moment originating from bacteriorhodopsin. It has been found that purple membrane is less charged than white membrane and the charge density of white membrane is different from that of white membrane with retinal [9]. Then, if the charge density has some influence on the flexibility of purple membrane, we could extract more useful information about the flexibility by comparing the dynamic behavior of purple membrane, white membrane and white membrane with retinal. It is quite interesting to investigate whether there is any difference in their dynamic behavior when the photochemical cycle is involved. This kind of study will be reported in the near future.

5. Conclusions

We have measured the spectrum of light quasi-elastically scattered from suspensions of purple membrane and discussed the characteristic behavior of correlation functions, especially the behavior of $\bar{\Gamma}/K^2$ against K^2. The apparent diffusion coefficient $\bar{\Gamma}/K^2$ showed quite specific features and did not increase monotonically with K^2 but showed distinct anomaly in the intermediate range of K^2 values. This behavior of $\bar{\Gamma}/K^2$ was well explained by a model for a disc-like scatterer. The diffusion coefficient D_0 was determined from the analysis of low-angle correlation functions, and the estimated size of membrane by the aid of Perrin's formula for D_0 was comparable to that from electron micrographs. The experimental $\bar{\Gamma}/K^2$ values, however, could not be explained quantitatively well by the model for a disc-like scatterer with the Perrin values of D_1, D_3 and Θ. Apart from a possible contribution of membrane flexibility, difficulties in a quantitative analysis of the experimental results came from two major sources, one being the size distribution of the scatterers and the other is that the purple membrane could not be completely modeled by a perfect disc because of its more or less irregular and elliptic circumferential shape. To examine the effect of polydispersity, a Schulz-Zimm distribution function was assumed, and it was found that the consideration of polydispersity alone could not sufficiently improve the discrepancy between experimental and theoretical results. To overcome the latter difficulty, we assumed a model for an extremely oblate ellipsoidal shell of revolution and obtained a qualitatively good agreement. A mixture of the two models for a disc and an ellipsoidal

shell may well explain the result, though the relative weight of these models could not be determined unequivocally because of the polydispersity and membrane flexibility. The relative weight of the models for a shell to a disc may not be large, because a large contribution from a shell results in a poor agreement between experimental and theoretical results at $K^2 \lesssim 2 \times 10^{10}\ \mathrm{cm}^{-2}$ (see fig. 9). Large deviations at larger K^2 values might arise from the contribution of membrane flexibility. Since, however, T/η scaling held well for the present system, we could not obtain obvious evidence of the contribution of membrane flexibility to the light-scattering spectra. Detection of membrane flexibility by dynamic light scattering may be possible by investigating purple membrane under various solvent conditions and by examining differences between the dynamic behavior of purple membrane and white membrane, for example, in order to avoid the above-mentioned difficulties. For this aim, a more sophisticated formulation is also required than that summarized in section 2 [7].

Though the results are not complete at present in both this study and the accompanying paper [7], they are believed to be the first to show the feasibility of membrane studies by dynamic light scattering.

Appendix: Algorithm on average of $\bar{\Gamma}/K^2$ over size distribution

For a polydisperse preparation, we have from eq. 6

$$\langle G^1(\tau)\rangle = \sum_n \sum_m (2m+1) \times \langle \left[U \exp\{ -(D_1 K^2 + \Theta\Lambda)\tau \} U^{-1} \right]_{nm} \times a_n(X) a_m(X) \rangle \qquad \text{(A1)}$$

where eq. 4 was used and $\langle \ldots \rangle$ denotes the average over a size distribution of scatterers. From the relationship $\bar{\Gamma} = -(\partial/\partial\tau) \ln G^1(\tau)|_{\tau=0}$, we have

$$\langle \bar{\Gamma} \rangle / K^2 = (3k_B T/32\eta) K \left[\langle 1/X \rangle_h + G_1(X) + G_2(X) \right] \qquad \text{(A2)}$$

where eq. 17 was used, $X = KR$ and

$$\langle 1/X \rangle_h = \left[\sum_n (2n+1) \langle a_n(X)^2/X \rangle \right] / \langle G^1(0) \rangle$$

$$G_1(X) = \left[\sum_n n(n+1)(2n+1) \langle a_n(X)^2/X^3 \rangle \right] / \langle G^1(0) \rangle$$

$$G_2(X) = -(1/3) \Big[\sum_n (2n+1) \langle a_n(X)/X \times \{ L_0(n) a_n(X) + L_2(n-2) a_{n-2}(X) + L_1(n+2) a_{n+2}(X) \} \rangle \Big] / \langle G^1(0) \rangle$$

$$\langle G^1(0) \rangle = \sum_n (2n+1) \langle a_n(X)^2 \rangle$$

Average quantities $G_1(X)$ and $G_2(X)$ should be compared with $g_1(X)$ and $g_2(X)$ in the text, respectively. A Schulz-Zimm distribution function, eq. 19, can be written as

$$W(z) = W(R)/W(\bar{R}) = [z \exp(1-z)]^m \times \exp(1-z)$$

where $z = R/\bar{R}$. Since we regard $W(z)$ as the number distribution function [24], we have for a disc system

$$\langle f(X) \rangle = \int_0^\infty f(\bar{X}z) z^4 W(z) \mathrm{d}z \Big/ \int_0^\infty z^4 W(z) \mathrm{d}z$$

where $\bar{X} = K\bar{R}$. For example, $\langle 1/X \rangle_h$ can be computed by

$$\langle 1/X \rangle_h = (1/\bar{X}) \times \sum_n (2n+1) \int_0^\infty z^3 a_n(\bar{X}z)^2 W(z) \mathrm{d}z \Big/ \sum_n (2n+1) \int_0^\infty z^4 a_n(\bar{X}z)^2 W(z) \mathrm{d}z$$

Since $(k_B T/12\eta)\langle 1/R \rangle_h^o = \langle D_0 \rangle_h^o$ where superscripts 'o' denote quantities at $K^2 \to 0$, we have

$$(k_B T/12\eta) K \langle 1/X \rangle_h^o = \langle D_0 \rangle_h^o \qquad \text{(A3)}$$

At $K^2 \to 0$ or $\bar{X} \to 0$, we have $a_0(\bar{X}) \to 1$ and

$a_n(\bar{X}) \to 0$ for $n \geqslant 2$. Then we have

$$K\langle 1/X\rangle_h^\circ = \langle 1/R\rangle_h^\circ$$
$$\to (1/\bar{R})\int_0^\infty z^3 W(z)\mathrm{d}z / \int_0^\infty z^4 W(z)\mathrm{d}z$$
$$= [(m+1)/(m+4)](1/\bar{R})$$

Since the Perrin value of $\langle 1/R\rangle_h^\circ$ can be determined from the experimental $\langle D_0\rangle_h^\circ$ value by use of eq. A3, $(295\ \mathrm{nm})^{-1}$ for sample A for example, we can determine the parameter value $\bar{R}$ of the distribution function experimentally.

In an actual computation of various average quantities, the integration over z was replaced by a summation over 100 points between z_L and z_H where $W(z_L) = W(z_H) = 0.01$. In the case of an extremely oblate ellipsoidal shell of revolution, $a_n(X)$ in the above equations should be replaced with $d_n^s(X)$.

Computed results are shown in fig. 9 for $\langle\bar{\Gamma}\rangle/K^2$ and in fig. 12 for $K^2\langle G^1(0)\rangle$ α

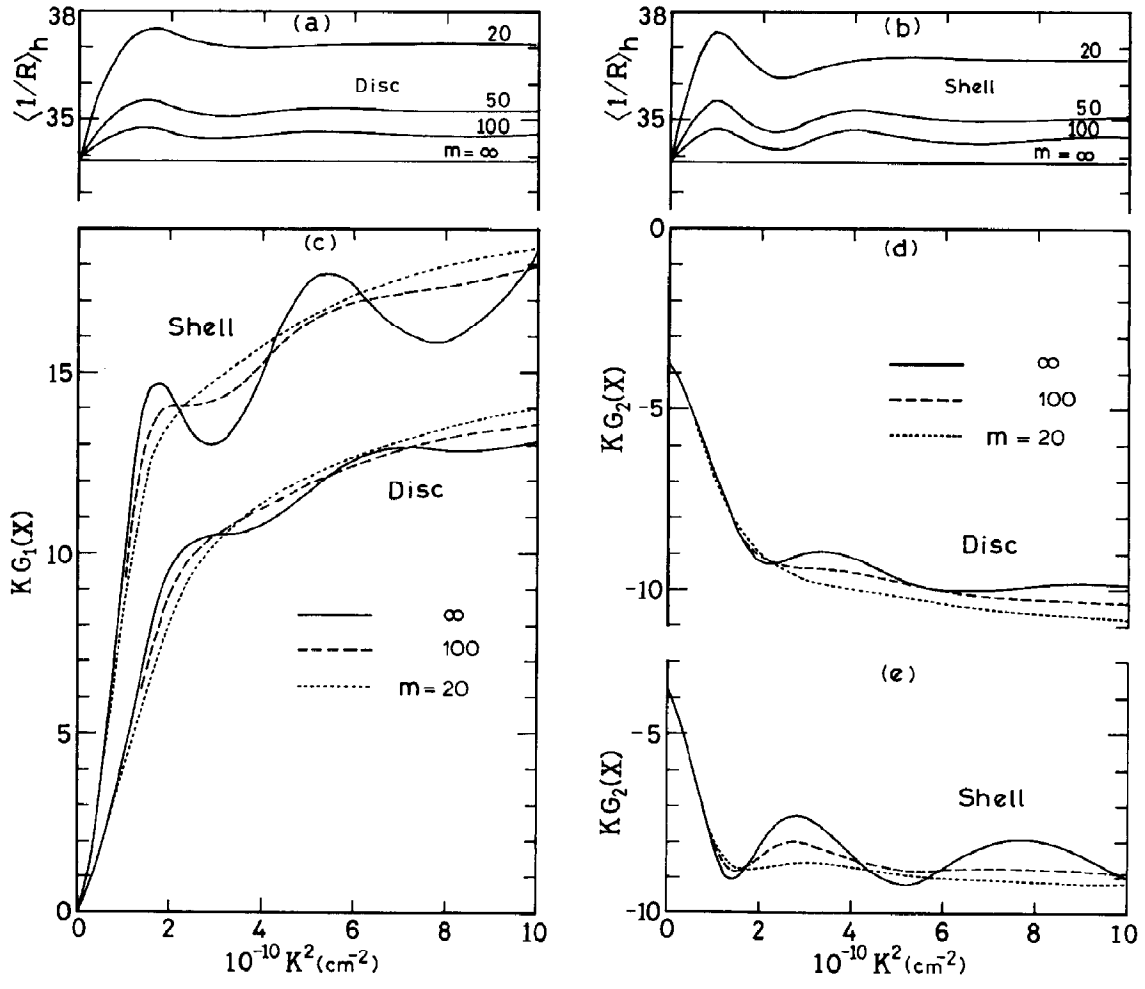

Fig. 13. Numerical results of simulation of the effect of size distribution on the component of $\langle\bar{\Gamma}\rangle/K^2$ for a disc (Disc) and an extremely oblate ellipsoidal shell (Shell). The ordinate is scaled in units of $10^3\ \mathrm{cm}^{-1}$, which can be converted to usual units of 10^{-8} cm^2/s by multiplying by $(3k_BT/32\eta) = 4.332\times10^{-13}\ \mathrm{cm}^3/\mathrm{s}$ at 25°C. $\langle 1/R\rangle_h^\circ = (295\ \mathrm{nm})^{-1}$ was assumed.

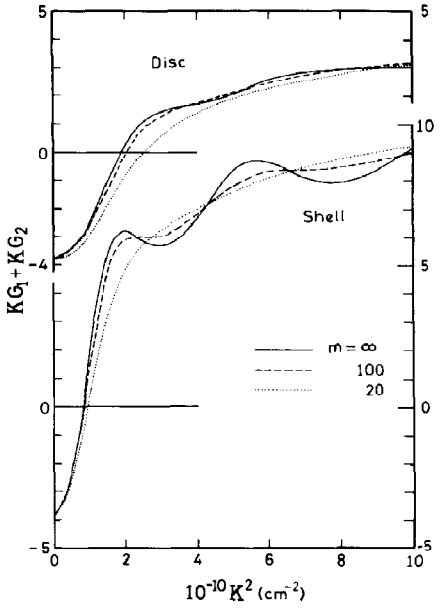

Fig. 14. Graphic representation of $K[G_1(X)+G_2(X)]$ for a disc (Disc) and an extremely oblate ellipsoidal shell (Shell). Units of ordinate and the assumed value of $\langle 1/R\rangle_h^\circ$ are the same as those in fig. 13.

$\sin^2(\theta/2)\langle I(\theta)\rangle$. Here, we would like to discuss briefly $\langle\bar{\Gamma}\rangle/K^2$. Apart from a factor $(3k_BT/32\eta)$, $\langle\bar{\Gamma}\rangle/K^2$ in eq. A2 is composed of three terms, $K\langle 1/X\rangle_h = \langle 1/R\rangle_h$, $KG_1(X)$ and $KG_2(X)$, of which numerical values are shown in fig. 13. For both models, polydispersity smears out wiggling in $KG_1(X)$ and $KG_2(X)$ and increases the values of $KG_1(X)$ and $|KG_2(X)|$ on average. However, because of $KG_1(X) > 0$ and $KG_2(X) < 0$, the sum $K[G_1(X)+G_2(X)]$ is less dependent on polydispersity (fig. 14). On the other hand, polydispersity definitely increases the value of $\langle 1/R\rangle_h$ at $K \neq 0$. Roughly speaking, an overall increase of $\langle\bar{\Gamma}\rangle/K^2$ with polydispersity (see fig. 9) is due to the increase in $\langle 1/R\rangle_h \propto \langle D_1\rangle_h$ values. An increase of $\langle 1/R\rangle_h$ by 3% or $1.0\times10^3\,\mathrm{cm}^{-1}$ at $K^2 \geqslant 1\times10^{10}$ cm^{-2} (fig. 13a) corresponds to the increase of D_1 by $0.043\times10^{-8}\,\mathrm{cm}^2/\mathrm{s}$, which attains almost 8% of the excess value of $\bar{\Gamma}/K^2$ at $K^2 = 10\times10^{10}$ cm^{-2}, i.e., $\bar{\Gamma}/K^2 - \langle D_0\rangle_h^\circ = (1.84-1.30)\times10^{-8}$ $= 0.54\times10^{-8}\,\mathrm{cm}^2/\mathrm{s}$ at $K^2 = 10\times10^{10}\,\mathrm{cm}^{-2}$.

Acknowledgements

We thank Dr. A. Tomioka of the University of Tokyo for kindly taking electron micrographs of our samples, Professor F. Kitahara of the Science University of Tokyo for permission to use his argon ion laser and Dr. H. Urabe for useful comments. This work was partly supported by Grant-in-Aid from the Ministry of Education, Science and Culture of Japan.

References

1 B. Chu, Laser light scattering (Academic Press, New York, 1974).
2 B. Berne and R. Pecora, Dynamic light scattering (Interscience, New York, 1975).
3 S.-H. Chen, B. Chu and R. Nossal, Scattering techniques applied to supramolecular and nonequilibrium systems (Plenum Press, New York, 1981).
4 J.C. Earnshaw and M.W. Steer, The application of laser light scattering to the study of biological motion (Plenum Press, New York, 1983).
5 T. Maeda and S. Fujime, Macromolecules 17 (1984) 1157.
6 K. Kubota, H. Urabe, Y. Tominaga and S. Fujime, Macromolecules 17 (1984) 2096, where $Y_m(I)^2$ in eq. 16 should read $[Y_m(I)-Y_c(I)]^2$.
7 S. Fujime and K. Kubota, Biophys. Chem. 23 (1985) 1.
8 T. Norisuye, W.F. Hoffman and H. Yu, Biochemistry 15 (1976) 5678.
9 L. Packer, B. Arrio, G. Johnnin and P. Volfin, Biochem. Biophys. Res. Commun. 122 (1984) 252.
10 D. Oesterhelt and W. Stoeckenius, Proc. Natl. Acad. Sci. U.S.A. 70 (1973) 2853.
11 R. Henderson, Annu. Rev. Biophys. Bioeng. 6 (1977) 87.
12 T. Norisuye and H. Yu, Biochim. Biophys. Acta 471 (1977) 436.
13 F. Perrin, J. Phys. Radium 5 (1934) 497.
14 D. Oesterhelt and W. Stoeckenius, Methods Enzymol. 31 (1974) 667.
15 Y. Kimura, M. Fujiwara and A. Ikegami, Biophys. J. 45 (1984) 615.
16 D.E. Koppel, J. Chem. Phys. 57 (1972) 4814.
17 S. Fujime and T. Maeda, Macromolecules 18 (1985) 191.
18 J. Newman and F.D. Carlson, Biophys. J. 29 (1980) 37.
19 T. Maeda and S. Fujime, Macromolecules 14 (1981) 809.
20 S. Fujime and T. Maeda, Biophys. J. 38 (1982) 213.
21 E.O. Schulz-Dubois, Photon correlation techniques in fluid mechanics (Springer-Verlag, Berlin, 1983).
22 G.V. Schulz, J. Phys. Chem. B43 (1939) 25.
23 B.H. Zimm, J. Chem. Phys. 16 (1948) 1099.
24 S.R. Aragón and R. Pecora, J. Chem. Phys. 64 (1976) 2395.